Feature-Based Generalized Gaussian Distribution Method for NLoS Detection in Ultra-Wideband (UWB) Indoor Positioning System

Fuhu Che, Qasim Zeeshan Ahmed, Jaron Fontaine, Ben Van Herbruggen, Adnan Shahid, Eli De Poorter, and Pavlos I. Lazaridis

***Abstract*— Non-Line-of-Sight (NLoS) propagation condition is a crucial factor affecting the precision of the localization in the Ultra-Wideband (UWB) Indoor Positioning System (IPS). Numerous supervised Machine Learning (ML) approaches have been applied for NLoS identification to improve the accuracy of the IPS. However, it is difficult for existing ML approaches to maintain a high classification accuracy when the database contains a small number of NLoS signals and a large number of Line-of-Sight (LoS) signals. The inaccurate localization of the target node caused by this small number of NLoS signals can still be problematic. To solve this issue, we propose feature-based Gaussian Distribution (GD) and Generalized Gaussian Distribution (GGD) NLoS detection algorithms. By employing our detection algorithm for the imbalanced dataset, a classification accuracy of 96.7% and 98.0% can be achieved. We also compared the proposed algorithm with the existing cutting-edge such as Support-Vector-Machine (SVM), Decision Tree (DT), Naive Bayes (NB), and Neural Network (NN), which can achieve an accuracy of 92.6%, 92.8%, 93.2%, and 95.5%, respectively. The results demonstrate that the GGD algorithm can achieve high classification accuracy with the imbalanced dataset. Finally, the proposed algorithm can also achieve a higher classification accuracy for different ratios of LoS and NLoS signals which proves the robustness and effectiveness of the proposed method.**

***Index Terms*— Ultra-wideband (UWB), Indoor Positioning System (IPS), Machine Learning (ML), Non-Line-of-Sight (NLoS) Identification, Gaussian Distribution mixture models, Generalized Gaussian Distribution (GGD).**

I. Introduction

With the rapid development of the Internet of Things (IoT)s, the requirement of a precise indoor positioning system (IPS) has attracted considerable attention in the research community and industry [1]–[7]. Several examples aforesaid, pedestrian tracking systems [4], [8], [9], autonomous flying drones in warehouses [9]–[11], and social distancing requirements caused by pandemic such as COVID-19 [13], [14], etc., require accurate IPS. The Global Navigation Satellite System (GNSS) provides tremendous convenience to human life as they provide real-time localization in open space. Unfortunately, the GNSS signals are attenuated severely by the wall and fail to achieve the accurate positioning in indoor environments [2], [15]. Among various indoor positioning technologies, Ultra-wideband (UWB) can achieve high accuracy due to its characteristics of extremely short pulse that provides good time resolution [6], [9], [16]. However, the accuracy of UWB IPS could be significantly affected when the NLoS signal occurs [12], [17], [18]. The NLoS condition exists when the signals between the transceivers are reflected or blocked by the obstacles. In this case, signal propagation delay occurs, resulting in longer Time-of-Flight (ToF) and an estimated distance error between the transmitter and receiver [17], [18]. Thus, significantly reducing the accuracy of IPS.

The current literature includes several research works that enhance the accuracy of the UWB IPS by identifying whether the signal has a LoS or NLoS component [9], [16], [17], [19]. The methods of NLoS identification can be coarsely summarised into two types (i) Non-feature based NLoS signal classification that uses context information and (ii) feature-based NLoS identification relying on the UWB waveforms. The *non-feature based approach* from [19] uses a modified Kalman filter to classify LoS/NLoS conditions based on the Bayesian sequential of range measurements. In [20], the authors present a real-time NLoS identification approach based on the received signal strength without the training phase and prior knowledge of the environment. In [21] models the NLoS as a deterministic additive term and identifies NLoS based on the statistical features of range measurements. In [22], a fusion technique such as an Inertial Navigation System (INS)

Part of the paper is also presented in 26th IEEE International Conference on Automation and Computing (ICAC), 2021. This work is supported in part by RECOMBINE-MSCA-Research and Innovation Staff Exchange (RISE)-2019 under Grant ID: 872857, the Capacity Building for Digital Health Monitoring and Care Systems in Asia EAC-A02-2019-CBHE under Grant ID: 619193, the Fund for Scientific Research Flanders, Belgium, FWO-Vlaanderen, FWO-SB, under Grant 1SB7619N, and the imec AAA UWB localisation research project 75.

Fuhu Che, Qasim Zeeshan Ahmed and Pavlos I. Lazaridis are with School of Computing and Engineering, University of Huddersfield, Huddersfield, UK (e-mail: q.ahmed@hud.ac.uk).

Jaron Fontaine, Ben Van Herbruggen, Adnan Shahid, Eli De Poorter are with IDLab, Department of Information Technology at Ghent University - imec, Belgium.

is combined with UWB for pedestrian tracking. In [9], the authors apply the floor map injunction with INS and UWB to predict the state and then determine and recognise the NLoS signals.

In contrast, in the *feature-based* NLoS *identification*, the UWB waveform signals under the LoS are different from those under NLoS conditions. These features can be extracted from the UWB signal to identify NLoS conditions by employing Machine Learning (ML) algorithms. One of the early ML-based NLoS identification approaches in UWB was proposing the Support Vector Machine (SVM) algorithm as a classifier in [23], [24]. In these papers [23]–[25], the identification of LoS and NLoS signals was considered as a binary classification problem. The results proved that the ML approaches could improve the accuracy of UWB IPS by identifying the NLoS signals. Different ML techniques like Naive Bayes (NB) [26], Boosted Decision Tree (BDT) [27], etc., were also investigated. Deep-learning based approach such as Convolutional Neural Network (CNN) was developed in [28]. Furthermore in [29], the authors propose a semi-supervised based ML approach using autoencoders which achieves 29% higher accuracy than state-of-the-art deep neural network algorithm. However, the above-mentioned feature-based methods have drawbacks, especially when the data is imbalanced and a small number of NLoS data samples are present. In such cases, it is hard for such algorithms to train a robust classifier for NLoS identification. To address this shortcoming, we propose a Gaussian Distribution (GD) and Generalized Gaussian Distribution (GGD) algorithms for NLoS signal detection in the presence of imbalance datasets. Our proposed GGD is an unsupervised learning algorithm. We start with the LoS data to build a training dataset, determine a threshold through density estimation according to the GGD of each feature, and test the classification of the new data according to this calculated threshold.

Therefore, the main contributions of this paper are as follows.

- Study the performance of an unsupervised learning algorithm based on Gaussian Distribution (GD) and Generalized Gaussian Distribution (GGD) algorithms to discriminate between LoS and NLoS conditions in presence of imbalance datasets with limited NLoS training data for IPS.
- Compare the proposed algorithm with the existing supervised ML algorithm (SVM, DT, NB, and NN) in terms of the confusion matrix, receiver operating characteristics (ROC) curve and the area under the curve (AUC) to show the superior performance of the proposed algorithms.

The remainder of this paper is organized as follows. Section III describes the overall UWB system model and the principle of UWB localization. In Section IV, our proposed classification algorithms are discussed. In Section V, the principle of our proposed algorithms is presented followed by the features used for NLoS signal classification. In addition, this section also discusses the environment in which the data was collected, and the hardware used for this data collection. Section VI presents the performance evaluation of the proposed algorithms and compare the results with the state-of-art ML algorithms in detail. The summary of the accomplishment is given in Section VII.

II. ABBREVIATIONS AND ACRONYMS

Angle-of-Arrival	- AOA
Area under the curve	- AUC
Additive White Gaussian Noise	- AWGN
Boosted Decision Tree	- BDT
Channel Impulse Response	- CIR
Conventional Neural Network	- CNN
Comma-Separated Value	- CSV
False Negative	- FN
False Positive	- FP
False Positive Rate	- FPR
Gaussian Distribution	- GD
Generalized Gaussian Distribution	- GGD
Global Navigation Satellite System	- GNSS
Inertial Navigation System	- INS
Internet of Things	- IoTs
Indoor Positioning System	- IPS
Line-of-Sight	- LoS
Import Vector Machine	- IVM
K-Nearest Neighbor	- KNN
Multi-Layer Perceptron	- MLP
Naïve Bayes	- NB
Non-Line-of-Sight	- NLoS
Probability Distribution Function	- PDF
Receiver Operating Characteristics	- ROC
Support Vector Machine	- SVM
Time-of-Arrival	- ToA
Time-of-Flight	- ToF
True Positive	- TP
True Positive Rate	- TPR
Ultra-wideband	- UWB

III. UWB Positioning System Model

A. Transmitted UWB Signal by the Anchor

We consider an UWB signal waveform $s(t)$ transmitted by the help of K pulses p with a period of T_p that consists of transmitted frames [30]. As the transmitted UWB signal location is known the transmitted signal is modelled as

$$s(t) = \sqrt{E_s} \sum_{k=1}^{K-1} p(t - kT_p), \tag{1}$$

where E_s is the energy of the UWB signal $s(t)$.

B. Received UWB Signal by the Mobile Node

The transmitted signal $s(t)$ experiences multipath channel effects and the received signal at the i-th mobile node can be expressed as [31], [32].

$$r_i(t) = \sum_{v_i=1}^{V_i} h_{v_i} s(t - \tau_{v_i}) + n(t), \quad i = 1, 2, \cdots, N. \tag{2}$$

where V_i is the maximum number of multipath experienced by the i-th mobile node. h_{v_i} and τ_{v_i} represent the amplitude and delay of the v-th path respectively at the i-th mobile node, and $n(t)$ is the Additive White Gaussian Noise (AWGN) with zero mean and two-sided power spectral density $N_0/2$. However, as this i-th mobile node or referred to a tag in literature will be moving, therefore, our main interest will be to calculate the distance between anchor node and the i-th mobile node. The distance calculation is discussed in the upcoming subsection.

C. Localization System

UWB-based IPS consists of two different kinds of nodes. Nodes with a known position are called anchors whereas the nodes with unknown position are tags and their position is to be determined. Firstly, time of arrival (ToA) technique can be used to measure the distance between the anchor and tag. Secondly, the triangulation technique helps to determine the position of the tag in a 2-dimensional ($2D$) environment with three or more than three anchors.

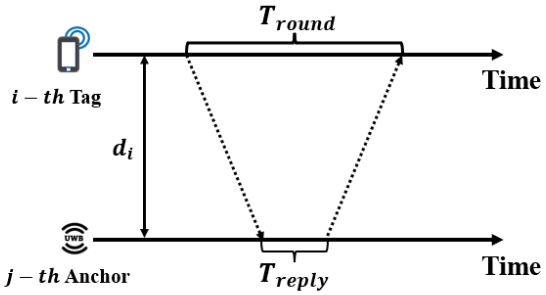

(a) Propagation time calculations

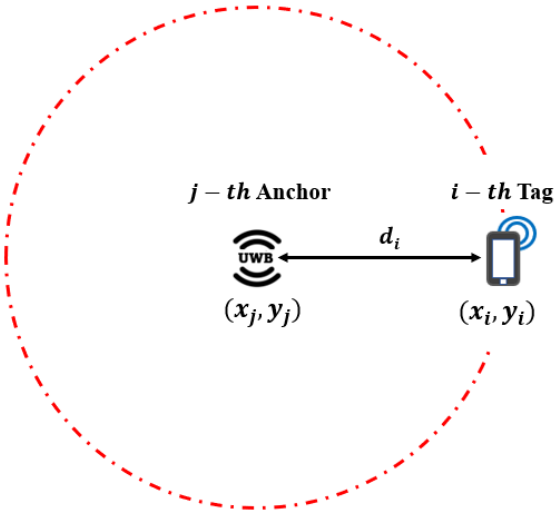

(b) Range scheme

Fig. 1: UWB localization theory in a 2-dimensional ($2D$) environment

1) Time of Arrival (ToA) Approach
The first process of ToA will require both the anchor and the tag to have synchronized clocks. As shown in Fig. 1a, a timestamp will be sent by the i-th tag to the j-th anchor. The timestamp will be processed by the j-th anchor in T_{reply} seconds and send back to the i-th tag. The time taken for the i-th tag is T_{round} and the propagation time $\tau_{\mathrm{i,j}}$ can be expressed as

$$\tau_{i,j} = \frac{T_{round} - T_{reply}}{2}, \quad i = 1, 2, \cdots, N, j = 1, 2, 3. \tag{3}$$

The estimate distance $d_{i,j}$ between the i-th anchor and j-th tag can be calculated as

$$d_{i,j} = c \times \tau_{\mathrm{i,j}}, \tag{4}$$

where c is the speed of light in meter per seconds (m/s). Fig. 1b shows the distance between the i-th tag and the j-th anchor. However, the coordinates of the tag will be unknown and for that the trilateration approach is required.

2) Trilateration Approach for UWB Localization
Fig. 1b shows the position of the i-th tag with respect to the j-th anchor. The coordinates of the j-th anchor are (x_j, y_j) which are already known. The coordinates of the i-th tag are represented as $(\hat{x}_i, \hat{y}_i)$, where $(\hat{\cdot})$ indicates the estimate of the position. The distance between each anchor and the tag is calculated as

$$d_{i,j} = \sqrt{(\hat{x}_i - x_j)^2 + (\hat{y}_i - y_j)^2}, \qquad i = 1, 2, \cdots, N, \; j = 1, 2, 3. \tag{5}$$

The position of tag $(\hat{x}_i, \hat{y}_i)$ can be determined by employing the least-squares solution.

IV. Proposed Algorithms

We are given a UWB training set of size TL such that $\mathcal{S} = \{\boldsymbol{s}_1, \boldsymbol{s}_2, \cdots, \boldsymbol{s}_{TL}\}^T$. If t represents the index of the dataset $\mathcal{S}$, then t will consist of M features and will be represented as $\boldsymbol{s}_t = \{s_{t,1}, s_{t,2}, \cdots, s_{t,M}\}$. The collection of these features are discussed in detail in the upcoming Section V. Upon collection of these features, we need to design ML algorithms such that we can classify the test data $\boldsymbol{u}_i$ of the i-th tag as LoS or NLoS signals. After training the dataset on the developed positioning algorithms we could classify the output of the test data $\boldsymbol{u}_i$ as $\{l = 0 \text{ or } 1\}$. This classification will indicate the LoS $l = 0$ or NLoS $l = 1$ status of the received signal. Let us now discuss the proposed positioning algorithms in detail.

A. Gaussian Distribution (GD)

Assuming the feature s_m to be Gaussian Distribution (GD) with mean μ_m, and variance σ_m^2 can be written as

$$P(s_m, \mu_m, \sigma_m^2) = \frac{1}{\sqrt{2\pi}\sigma_m} \exp\left(-\frac{(s_m - \mu_m)^2}{2\sigma_m^2}\right), \quad m = 1, 2, \cdots, M. \tag{6}$$

However, we will still require to calculate the mean μ_m and the variance σ_m^2 of the m-th feature. As the exact mean and variance of the features of the dataset is unknown, we can incorporate the provided training data TL to calculate their

estimates. The estimate of the mean $\hat{\mu}_m$ and variance $\hat{\sigma}_m^2$ for the m-th feature can be calculated as

$$\hat{\mu}_m = \frac{1}{TL}\sum_{t=1}^{TL} s_{t,m}, \quad m = 1, 2, \cdots, M, \tag{7}$$

$$\hat{\sigma}_m^2 = \frac{1}{TL}\sum_{t=1}^{TL} (s_{t,m} - \hat{\mu}_m)^2, m = 1, 2, \cdots, M. \tag{8}$$

Once we have the estimates of the mean and variance of each feature on training data, given a test data $\boldsymbol{u}_i$ we can calculate the probability as

$$P(\boldsymbol{u}_i) = \prod_{m=1}^{M} P(u_m, \hat{\mu}_m, \hat{\sigma}_m^2), \quad i = 1, 2, \cdots, N, \tag{9}$$

and classify the output as:

$$l = \begin{cases} P(\boldsymbol{u}_i) > \epsilon, & \text{LoS} \\ P(\boldsymbol{u}_i) \leq \epsilon, & \text{NLoS} \end{cases} \tag{10}$$

where ϵ is judgment boundary and will be discussed in detail in section V.

B. Generalized Gaussian Distribution, (GGD)

By using GD algorithm, some abnormal features of LoS data may be difficult to classify, as a result the model could wrongly classify it as a NLoS component. Furthermore, the GD algorithm require two key parameters to be modelled: a) mean and b) variance of the data as mentioned IV-A. In such cases, the GD model may not be able to accuracately identify the NLoS dataset. Therefore, instead of GD, Generalized Gaussian Distribution (GGD) can be adopted [30]. The GGD of the m-th feature can be written as

$$P(s_m, \mu_m, \alpha_m, \beta_m) = \frac{\beta_m}{2\alpha_m \Gamma(1/\beta_m)} \exp\left(-\frac{|s_m - \mu_m|}{\alpha_m}\right)^{\beta_m} \tag{11}$$

where μ_m is the mean, β_m determines the shape of the PDF, α_m is the scale parameter of the GGD and $\Gamma(\cdot)$ is the gamma function. The variance σ_m^2 and the kurtosis κ_m if the GGD is given as

$$\sigma_m^2 = \frac{\alpha_m^2 \Gamma(3/\beta_m)}{\Gamma(1/\beta_m)}$$

$$\kappa_m = \frac{\Gamma(5/\beta_m)\Gamma(1/\beta_m)}{\Gamma(3/\beta_m)^2} - 3. \tag{12}$$

Given a dataset $\mathcal{S}$, for GGD algorithm we need to estimate the mean $\hat{\mu}_m$, variance $\hat{\sigma}_m^2$ and kurtosis $\hat{\kappa}_m$ which are calculated as

$$\hat{\mu}_m = \frac{1}{TL}\sum_{t=1}^{TL} s_{t,m}, \quad m = 1, 2, \cdots, M, \tag{13}$$

$$\hat{\sigma}_m^2 = \frac{1}{TL}\sum_{t=1}^{TL} (s_{t,m} - \hat{\mu}_m)^2, \quad m = 1, 2, \cdots, M, \tag{14}$$

$$\hat{\kappa}_m = \frac{\frac{1}{TL}\sum_{t=1}^{TL} (s_{t,m} - \hat{\mu}_m)^4}{\left[\frac{1}{TL}\sum_{t=1}^{TL} (s_{t,m} - \hat{\mu}_m)^2\right]^2} - 3, m = 1, 2, \cdots, M, \tag{15}$$

where the estimate of kurtosis $\hat{\kappa}_m$ can be used to measure the shape parameter β_m and estimate of variance $\hat{\sigma}_m^2$ can help to determine the scale parameter α_m of the GGD. Now the test data $\boldsymbol{u}$ can be employed to calculate the probability as

$$P(\boldsymbol{u}_i) = \prod_{m=1}^{M} P(u_m, \hat{\mu}_m, \hat{\alpha}_m, \hat{\beta}_m), \quad i = 1, 2, \cdots, N. \tag{16}$$

where the classification can be done with the help of (10). For the sake of clarity, the GGD algorithm is summarised in the next subsection.

Algorithm 1 : Training Stage

Input: Collected dataset of UWB consisting of LoS and NLoS signal features.
Output: Create model $P(\boldsymbol{s}_i)$ for the i-th tag of the dataset $\mathcal{S}$.
Algorithm

1) Initialize and pre-process the dataset.
2) Select part of LoS as training data.
3) Estimate the mean $\hat{\mu}_m$,
4) Estimate the variance $\hat{\sigma}_m^2$, and
5) Estimate the kurtosis $\hat{\kappa}_m$,
6) Construct the model $P(s_m)$ for the m-th feature.
7) Select the threshold ϵ by calculating F_1-score value.
8) Construct the model $P(\boldsymbol{s}_i)$.

Algorithm 2 : Testing Stage

Input: Test dataset with a mixture of LoS and NLoS signals.
Output: Determine whether it is LoS or NLoS and then determine the exact location of the tag or the moving node.
Algorithm:

1) Fit the model by calculating the probability $P(\boldsymbol{u}_i)$ of the testing data as mentioned in (16).
2) **If** $P(\boldsymbol{u}_i) \leq \epsilon \leftarrow$ NLoS signal.
3) **Else** $P(\boldsymbol{u}_i) > \epsilon \leftarrow$ LoS signal.
4) Determine the distance between the tag and the respective anchor using (5).

C. Classification Algorithm

For the proposed classification technique, we first extract the LoS and NLoS signal features from the received dataset $\mathcal{S}$, then use distribution of each features to establish a model $P(\boldsymbol{s}_i)$ for the i-th tag. After the model is built and the threshold is selected, we fit this model with the test dataset $\boldsymbol{u}_i$ and classify whether the signal experiences a LoS or NLoS signal. The steps of the training and testing stage of the proposed GGD algorithm are shown in Algorithm 1 and 2, respectively. As GGD is the more generalised algorithm we have only summarised it. For GD algorithm step 5 will not be required in Algorithm 1. For Algorithm 2 in step-1 we will replace (16) with (9). Let us now look into the experimental setup followed by data collection, configuration of the UWB kit and key feature extractions in detail.

V. Experiment Setup

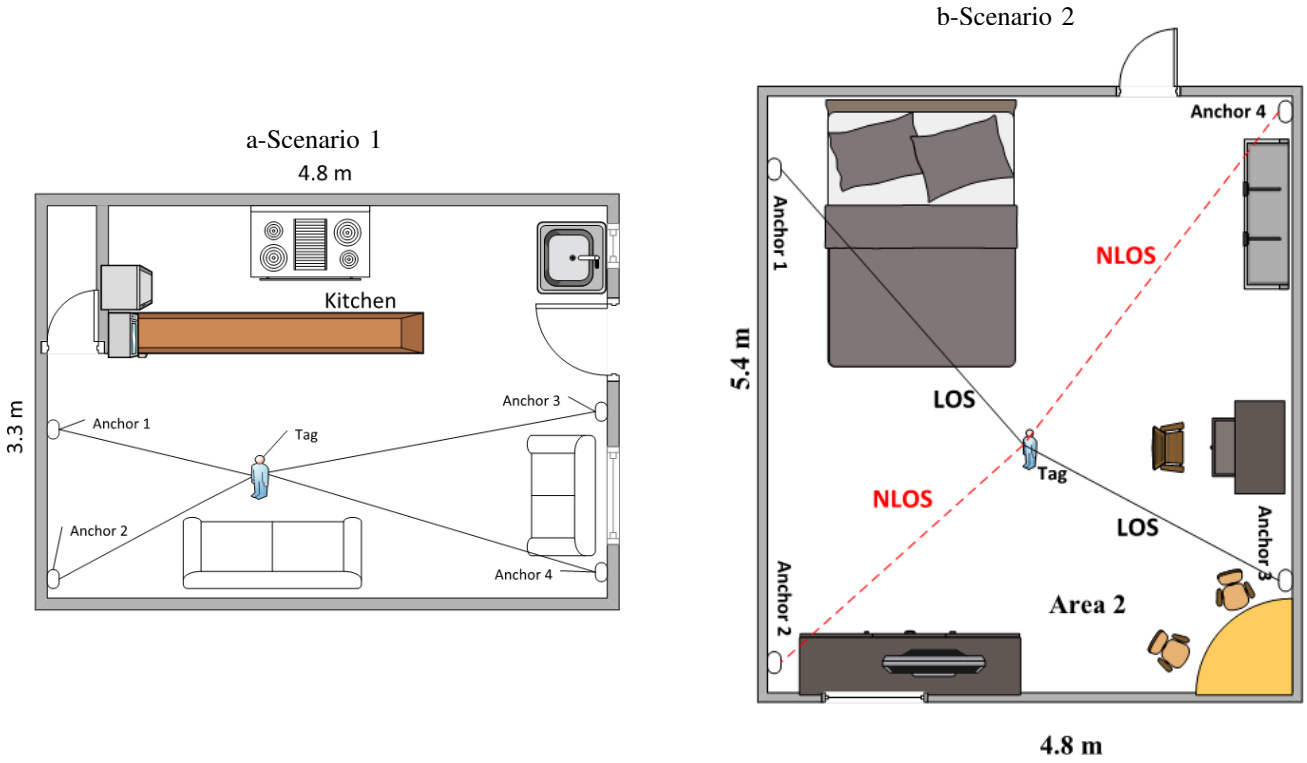

Fig. 2: The scenarios where training and test data were collected for evaluation:(a) Studio (b) Room

A. Data Extraction and Key Feature Selection Process

In this paper, MDEK-1001 UWB kits from DECAWAVE company are employed for data preparation. The configuration of the UWB kit is shown in Table I. All the experiment is carried out using MATLAB (R2020b). Two separately independent datasets for evaluation were collected in a small studio environment of dimensions (3.3×4.8) m as shown in Figure 2(a) and a room environment of size (4.8×5.4) m as shown in Figure 2(b). In this paper, we have utilised scenario-1, therefore, the studio environment for all the performance evaluation. For Table IV and Fig. 11 only scenario-2 is employed to observe the robustness of the proposed algorithms. During the LoS data collection, there was absolute clear environment between the anchors and tag. For NLoS data collection, there was an iron sheet placed between the anchors and the tag, so that no direct path of signal can be transmitted or received by it. The tag was connected to a PC and the data was logged via the Teraterm software into a comma-separated value (CSV) file. The collected dataset, had 15000 signals and 1000 LoS and 100 NLoS signals are collected randomly. This selection results in a ratio of $1 : 0.1$ for the LoS and NLoS signal. Finally, we randomly select different proportions of LoS and NLoS data to test the robustness of proposed algorithm.

For our analysis, 7 signal components are extracted that are:

1) Amplitude of the first path (F_1).
2) Amplitude of the second path (F_2).
3) Amplitude of the third path (F_3).
4) Preamble accumulation count value.

TABLE I: Configurations of the MDEK-1001 UWB kit.

Properties	Values
Chip	DW 1000
Transceiver	DWM1000
Pulse shape	Gaussian pulse
Number of Anchors	4
Data Rate	6.8 Mbps
Frequency	3993.6 MHz
Bandwidth	499.2 MHz
Channel	2
Pulse Repetition Frequency (PRF)	16 MHz

5) Amplitude of the channel impulse response (CIR).
6) Standard noise variance reported in the DW-1000 chipset.
7) The estimated calculated distance.

In brief, among the mentioned NLoS identification methods in the literature, the threshold difference between the first-path power and received power have been widely used in different ML algorithms [17], [33], [34]. In our analysis we will use the above 7 signal components to calculate our 4 key features which are the estimated distance (5), first path power level (17), received power level (18), and the power difference between the first and the received power level (19). The first-path power level is calculated as [17], [35]

$$\text{FP Level} = 10 \times \log_{10}\left(\frac{F_1^2 + F_2^2 + F_3^2}{N^2}\right) - A \quad \text{dBm}, \quad (17)$$

where F_1, F_2 and, F_3 represent first, second and third harmonics of the first-path signal amplitudes. A is a constant

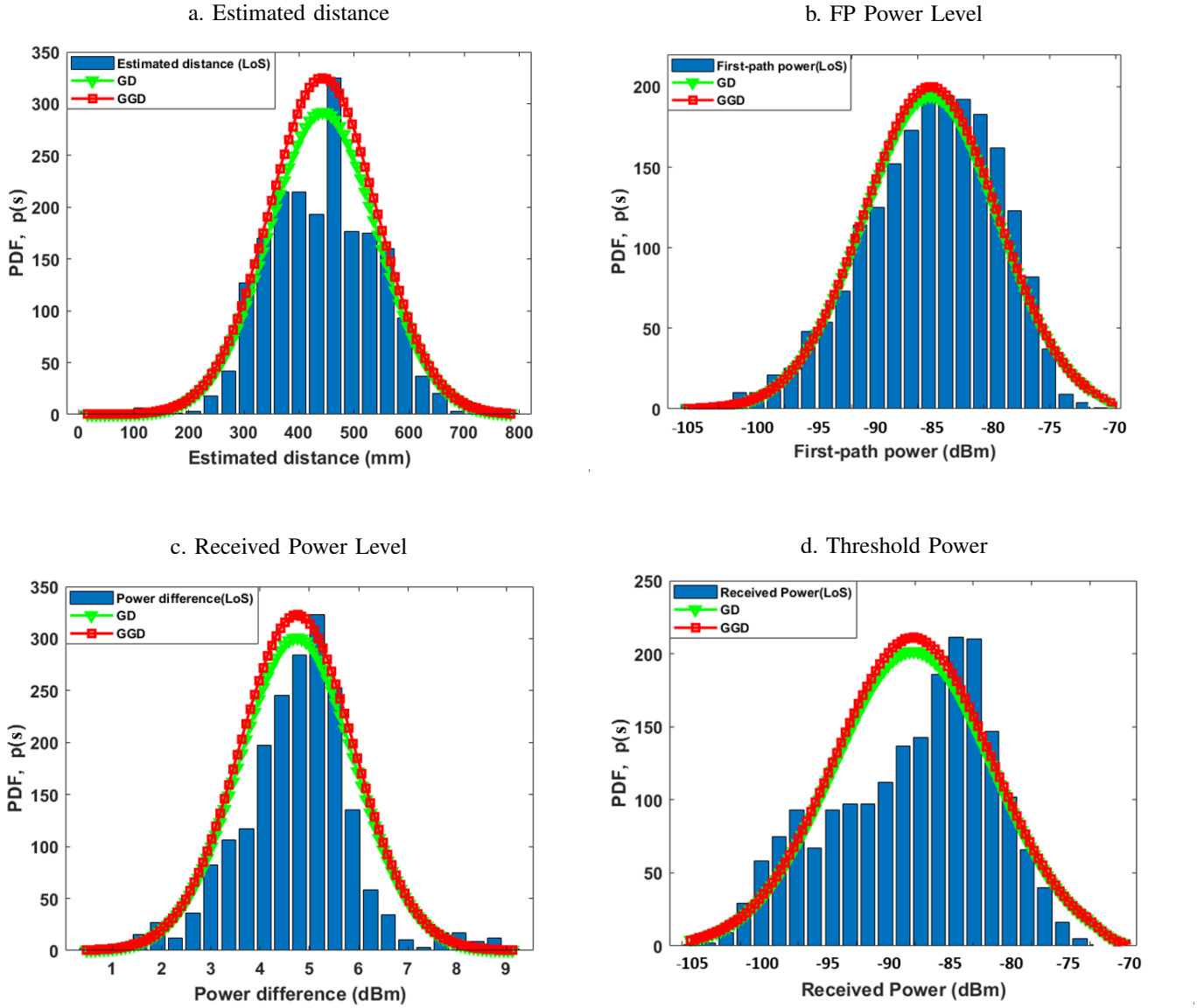

Fig. 3: Histogram distribution of our 4 key features in LoS environment a) Estimated distance, b) first path power level, c) received power level, and d) the threshold power.

equivalent to 113.77 when a PRF is 16 MHz as mentioned in [35] (page-46), and N is the Preamble Accumulation Count value. The received power level of the signal can be computed as [35]

$$\text{RX Level} = 10 \times \log_{10}\left(\frac{CIR \times 2^{17}}{N^2}\right) - A \quad \text{dBm}, \quad (18)$$

where CIR is the Channel Impulse Response Power value and 2^{17} is a correction factor so that the register value of DWM 1000 can be converted into the right magnitude for conversion into dBm. The power dissipation in NLoS environment is higher than the LoS environment due to multi-path effects, resulting in the first path of the LoS signal to have more power than the the first path of the NLoS signal. This knowledge can now be employed to improve the detection capability of the algorithm, therefore, the difference between the received and first-path power can also be employed. The formula is as shown in

$$\text{Threshold Power} = \text{RX Level} - \text{FP Level} \quad (19)$$

Figures 3 and 4 show the probability density function (pdf) of the selected four features which are the estimated distance, first-path power, received path power, and the power difference. Histogram function is employed to generate the pdfs of these features and are represented by the blue bars. The GD and GGD distribution is plotted by using the equation (9) and (16), respectively. For GD distribution, only mean and variance of the data is required. However, for GGD distribution, mean, variance, and kurtosis is required. The distribution of the features can be more closely approximated with the GGD as it has three parameters to update as compared to GD which only has two parameters. From these figures, it can be observed that the selected features follow GD and GGD distribution, therefore, the proposed algorithms can be used

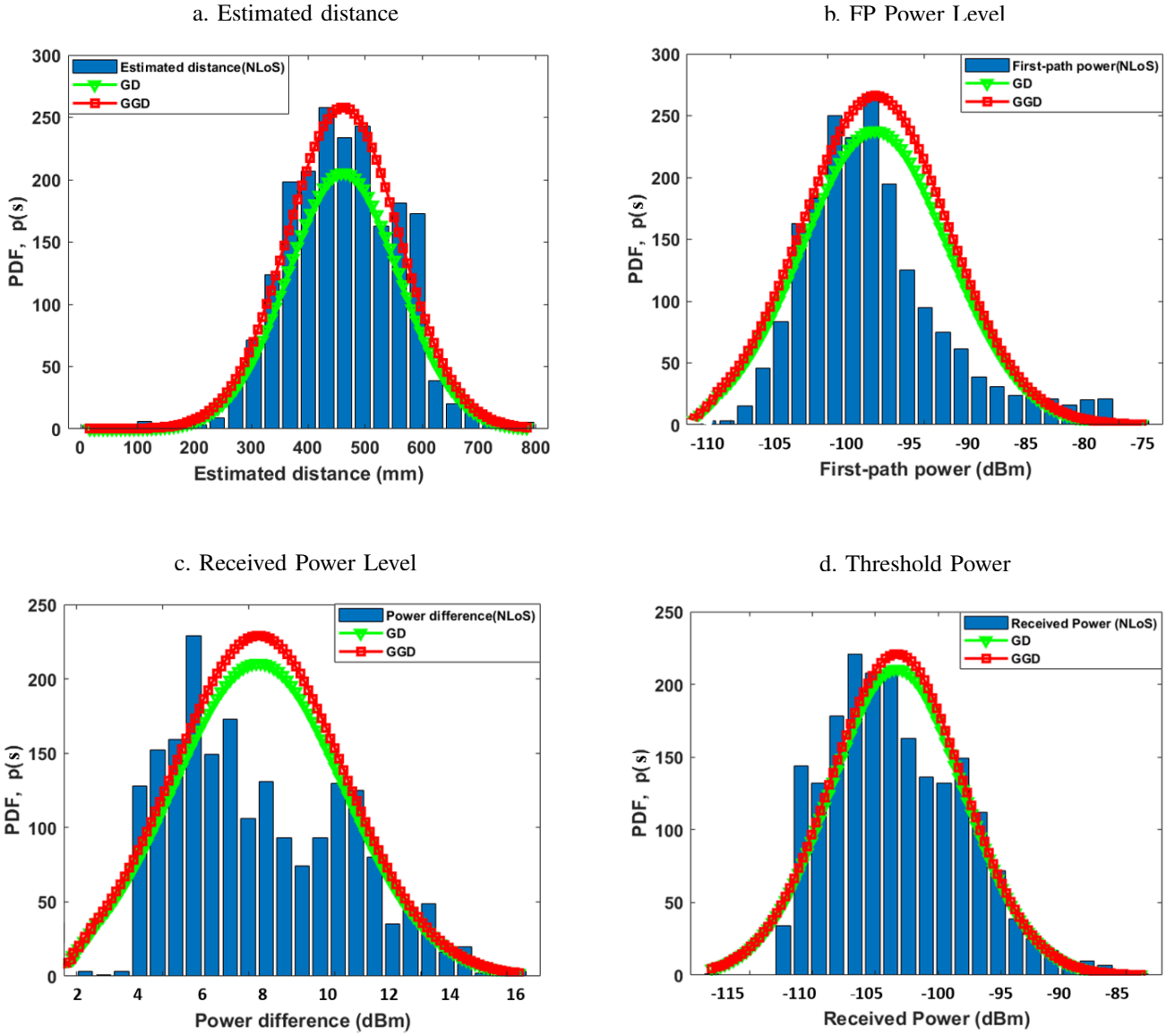

Fig. 4: Histogram distribution of our 4 key features in NLoS environment a) Estimated distance, b) first path power level, c) received power level, and d) the threshold power.

for the data classification. Let us now look into designing the selection threshold for these pdfs.

B. Threshold Selection, ϵ

In order to classify the LoS and NLoS signals, we need to select an appropriate threshold ϵ as mentioned in section IV. For threshold ϵ selection, we start by constructing a training set, then use the remaining LoS and NLoS signals to cross-check and validate the results, and finally carry out the testing as mentioned above. According to the training data set, we estimate the mean, variance, and kurtosis of each features to build function $P(\boldsymbol{s}_i)$ as mentioned in algorithm 1. The threshold ϵ was chosen based on the F-Score. F-Score is defined as the weighted average of precision and recall and calculated as

$$\text{F-Score} = \frac{2 \times (\text{Recall} \times \text{Precision})}{\text{Recall} + \text{Precision}}, \tag{20}$$

where Precision and Recall are defined as

$$\text{Precision} = \frac{TP}{TP + FP}, \tag{21}$$

$$\text{Recall} = \frac{TP}{TP + FN}, \tag{22}$$

where TP is the True Positive, FP is the False Positive, FN is the False Negative, and TN is the True Negative, respectively. TP means that the instances are classified as positive when they are actually positive, TN illustrates the instances are classified as negative when they are in negative condition. FP shows that the instances are classified as positive when they are negative. Similarly, FN represents the instances classified as negative when they are actually positive. However, the indoor environment changes and therefore, we have added a forgetting factor λ for the calculation of threshold ϵ. In such a case, the threshold can be updated after training and therefore can incorporate small changes in the environment.

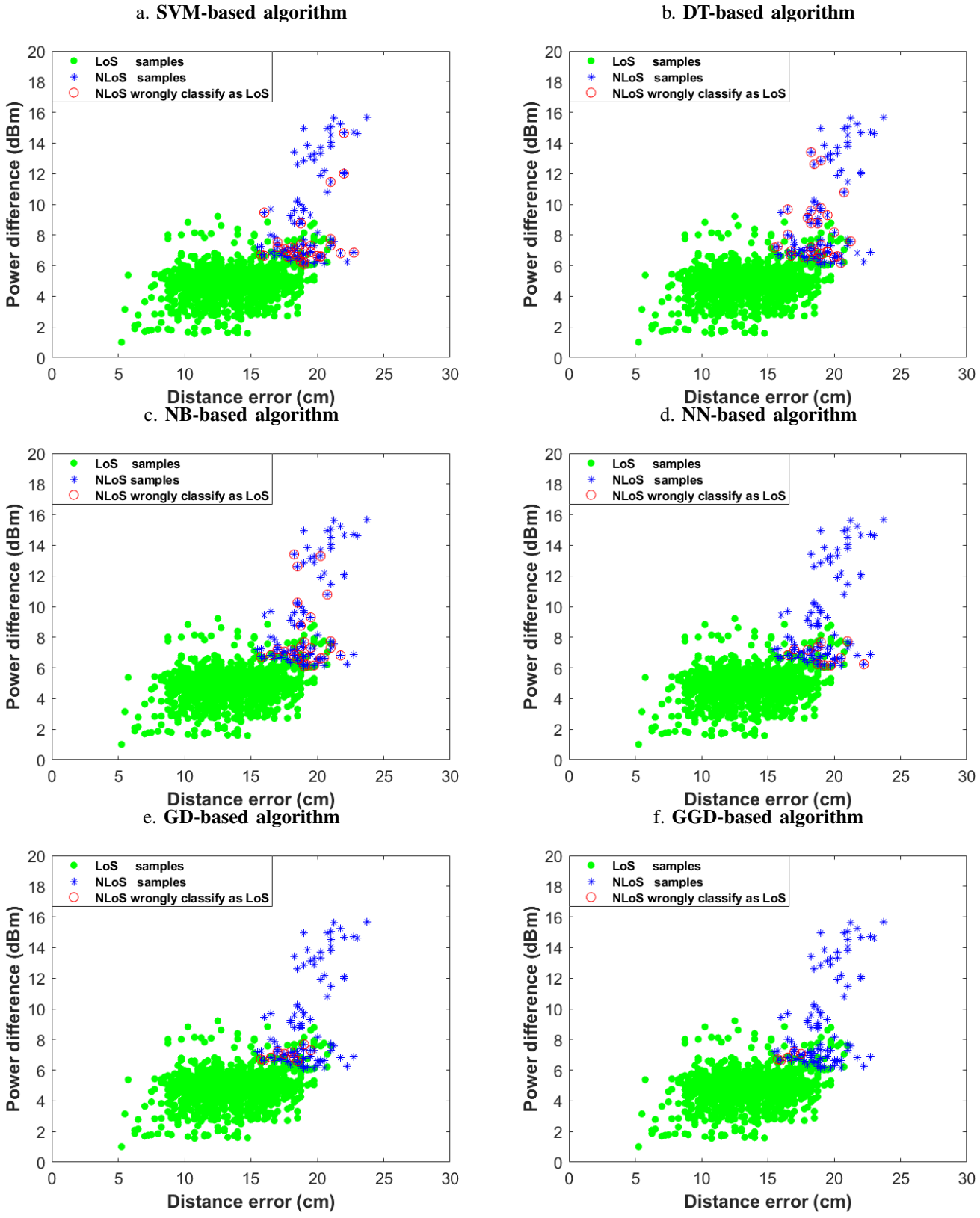

Fig. 5: Visualization of samples a) SVM-, b) DT-, c) NB-, d) NN-, e) GD-, and f) GGD-based algorithms.

The threshold can be updated by the following equation

$$\epsilon_{t+1} = \epsilon_t + \lambda \times e_t, \tag{23}$$

where t is the time index and e_t is the error if we classify the LoS as NLoS or vice versa. This will help us update the threshold after training.

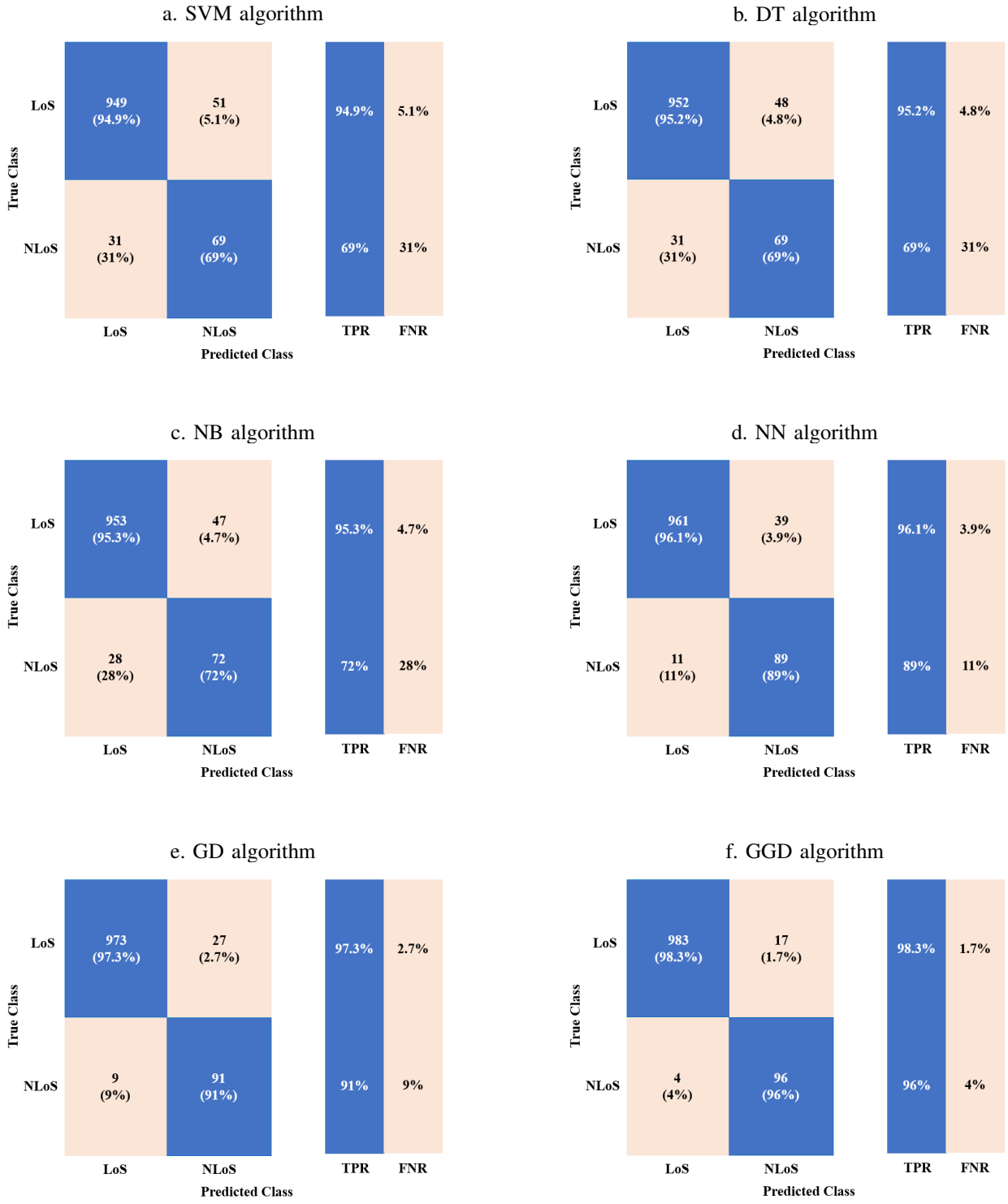

Fig. 6: The confusion matrix of the validation data set on six algorithms a) SVM, b) DT, c) NB, d) NN, e) GD, and f) GGD algorithms. The proposed algorithms improve the classification significantly.

VI. Performance Evaluation

In this section, we examine the performance of proposed algorithms. We first compare the results of the proposed classifier with the state-of-the-art machine learning algorithm based on SVM, DT, NB, and NN and start by computing two quantitative metrics: (i) confusion matrix that shows the classification results of each individual classifier, and (ii) Receiver Operating Characteristics (ROC) curve and corresponding Area-Under-the-ROC curve (AUC) value. Second, we calculate the performance of these algorithms in terms of precision, recall and accuracy. Third, the effect of different ratios of LoS and NLoS is studied for these algorithms and finally, the effect of change in environment to observe the robustness of our proposed algorithms.

The visualization of the samples are shown in Figure 5. The visualization of the samples is plotted with the help of the power difference calculated using (19) and the distance error that is calculated in centimeters. There are 1000 LoS and 100 NLoS signals, respectively. In this figure, the green samples represent the LoS signals and the blue colour represents the NLoS signals. The blue samples with red circle are the NLoS samples which have been falsely classified as LoS. It can be observed from these figures that the proposed GGD algorithm can provide a higher classification by setting an appropriate threshold by training the features as mentioned in section V as compared to the GD and the classical ML algorithms. For the SVM-, DT-, NB- and NN-based algorithms the performance is relatively poor as compared to GD and the GGD algorithm, this is due to the limited number of NLoS signals in the dataset failed to train a robust model for classification. Finally, it can be concluded that for imbalanced dataset the GD and GGD performs exceptionally better in classifying the LoS and NLoS signals as compared to conventional ML algorithms such as SVM-, DT-, NB-, and NN- based algorithms.

TABLE II: Dataset of the LoS and NLoS signals

Signal	Distance m	RX level dBm	FP level dBm	PD dBm	Classified
LoS	7.92	-92.72	-89.63	3.09	LoS
LoS	9.98	-94.16	-89.55	4.61	NLoS
NLoS	7.22	-95.27	-88.40	6.87	NLoS
NLoS	7.38	-93.96	-88.53	5.43	LoS

Table II shows an example of LoS and NLoS signal for the proposed UWB system. From the table it can be observed that we have distance and three features that are RX power level, FP power level, and PD power levels followed by how it is classified by the algorithm. From the table and as mentioned previously, the PD is more for NLoS signals as compared to LoS signals. However, still it cannot be simply employed for classification a signal as LoS or NLoS. Therefore, for accurate classification of an UWB system we will require a number of different features.

Figure 6 plots the confusion matrix of the four known ML algorithms (SVM, DT, ND, and NN) followed by the two proposed algorithms GD and GGD. All these algorithms are based on 1000 LoS and 100 NLoS signals. From these confusion metrics, it can be concluded that the worst performance in terms of True Positive Rate (TPR) for LoS components is achieved by SVM which is 94.9%. NB algorithm performs 0.01% better than DT in terms of TPR, however, NN algorithm achieves the best performance of 96.1% as compared to traditional ML algorithms. We can observe that the proposed GD and GGD performance is better than the existing ML algorithms and in terms of TPR in LoS components is 97.3% and 98.3%, respectively. Similarly, for NLoS components the performance of NN is much superior as compared to the SVM, DT, and NB. SVM and DT can correctly classify only 69% of NLoS components. NB classifies only 72% of TNs. NN can classify 89% while GD and GGD can classify more than 90% NLoS components accurately. Therefore, from Fig. 6 it can be observed that for both the LoS and NLoS components GD and GGD algorithms perform much superior to the classical ML algorithms such as SVM, DT, NB, and NN.

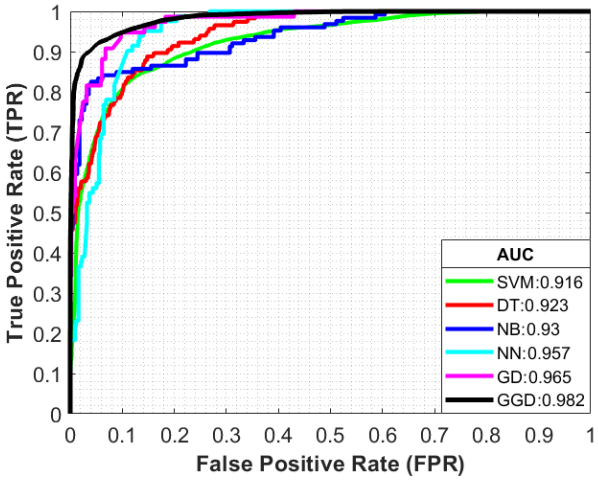

Fig. 7: Receiver Operating Characteristics (ROC) and Area under the curve (AUC) comparison of the algorithms

Figure 7 plots the receiver operating characteristics (ROC) curve. With these ROC curves, area under the curve (AUC) can be studied for the proposed and ML based positioning algorithms. The ROC curve is plotted with respect to the true positive rate (TPR) versus the false positive rate (FPR). Generally, in a ROC curve the best classifier is closer to the upper left corner, resulting in a larger AUC. From figure 7 it can be observed that the GGD algorithm is closer to the upper left corner as compared to other algorithms. Furthermore, the AUC of GGD algorithm is 0.982 which is more than any compared algorithm. As a result, the overall GGD algorithm will be superior in terms of classification accuracy as compared to other algorithms. The second best performance was achieved by the GD algorithm that was around 0.965 and the SVM performance was the worst despite achieving a value of 0.916. Out of all the ML algorithms NN performed superior as the area under the curve was equivalent to 0.957. Finally, it can be observed that the proposed algorithms, therefore GD and GGD, perform superior to the other ML algorithms as they can classify the data more accurately.

Figure 8 shows the evaluation results of these algorithms in terms of precision, recall, and accuracy. All these confusion matrices are formed by the help of 1100 classified samples consisting of 1000 LoS and 100 NLoS signals. From the figure, it can be observed that the accuracy of the SVM-based algorithm is equivalent to 92.6%. The accuracy of the DT-based, NB-based, and NN-based algorithms is 92.8%, 93.2%, and 95.5%, respectively. The GD-based algorithm results in more than 96.5%. The overall accuracy achieved with the GGD-based algorithm is around 98% which shows the GGD-based algorithm is superior to the classical ML and GD-based algorithms. Finally, Table III summarizes and represents the performance of all these algorithms in numbers. It can be observed from the table that GGD algorithm has superior TPR, TNR, Precision, Recall, Accuracy and AUC as compared to all the algorithms. Furthermore, the FPR and FNR are also the lowest as compared to GD and classical ML algorithms.

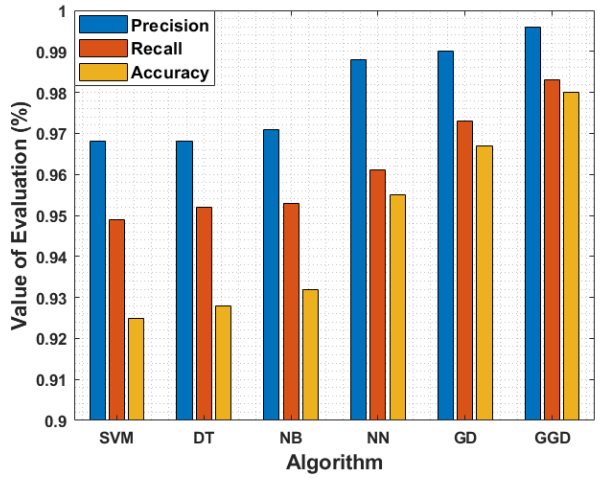

Fig. 8: Performance comparison in terms of Precision, Recall, and Accuracy.

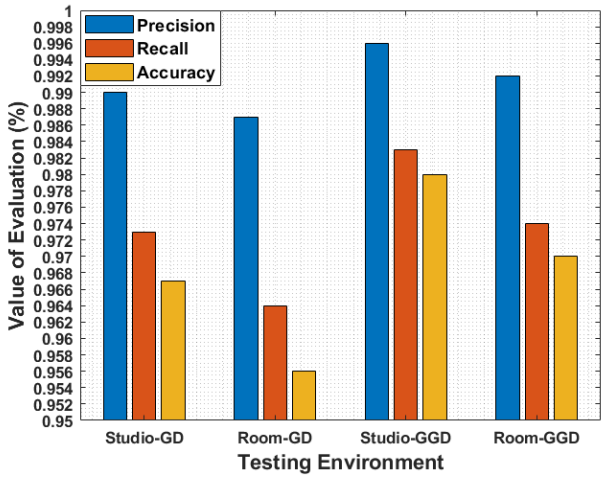

Fig. 10: Comparison of static and dynamic threshold ϵ

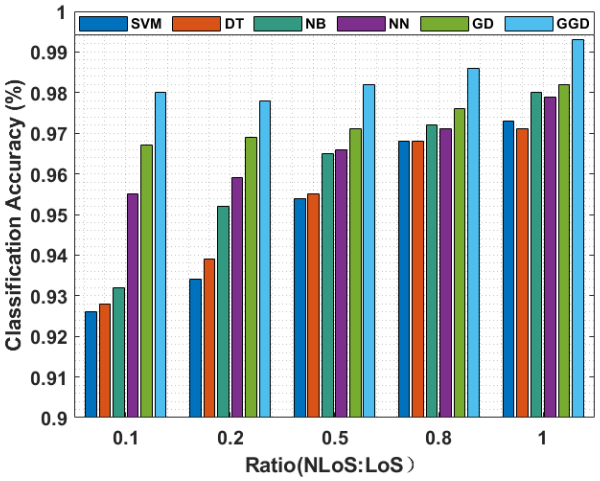

Fig. 9: Classification accuracy with different ratios of LoS and NLoS for different algorithms.

However, in this case, the accuracy of the algorithms is dominated by the LoS signals, therefore, in our next figure we observe the impact of increasing NLoS signals as compared to LoS signals.

Figure 9 graphically shows the classification accuracy of different ratios of LoS and NLoS samples for the classical ML, GD, and GGD algorithms. The reason for plotting this curve is to see the effect of the imbalanced dataset. From the figure, it can be observed that we have five different ratios $0.1, 0.2, 0.5, 0.8$, and 1.0, respectively. With a ratio of 0.1, we will have 1000 LoS and 100 NLoS signals. However, as the ratio increases the number of NLoS signals increases. Therefore, for a ratio of 1, we have 1000 LoS and 1000 NLoS signals. From the figure, it can be observed that the classification accuracy significantly improves as the ratio in the imbalanced datasets decreases. For the SVM algorithm, the improvement in classification accuracy performance is significantly more as compared to the other algorithms. For a ratio of 0.1, the accuracy is around 92.6%, while the maximum accuracy is achieved when we have a balanced dataset with a ratio of 1, therefore, around 97.2%. For the GD algorithm, the classification accuracy improves from 96.7% to 98% when the imbalance in the dataset is improved. Finally, for the GGD algorithm, the worst classification is around 98% and the best is around 99.3% for the balanced dataset. The total improvement in classification accuracy is around 3.6% for the SVM algorithm, 2.5% for the GD algorithm, and 1.5% for the GGD algorithm. This indicates that the GGD algorithm is more robust as compared to GD and NB algorithms for a given imbalanced or balanced dataset. Finally, this simulation result proves that the GD and GGD can guarantee better results for NLoS identification under different situations compared to the ML algorithms especially when the dataset is imbalanced.

Figure 10 shows the impact of the updating the threshold ϵ after every time instant. There are two approaches shown in the figure that are static and dynamic threshold ϵ approach. In the static-threshold approach, the ϵ is not updated after training and therefore can not update itself if there is any change in the environment. However, in the dynamic threshold approach the ϵ is updated after training by employing a forgetting factor $\lambda = 0.95$ as mentioned in (23). It can be observed from the figure that for both the GD and GGD algorithms, the dynamic threshold performs better than the static threshold. An improvement of approximately 0.04 and 0.02 is achieved in terms of accuracy by adopting the dynamic threshold approach as compared to static approach for GD and GGD algorithms. Therefore, in this paper dynamic threshold approach is employed.

In order to examine the proposed algorithm, we carried out experiments in two different scenarios as shown in Figure 11. The configuration of the UWB devices remained the same during the measurements. We build the UWB model using the studio dataset and then tested it on the room data-set. The results are shown in Table IV and plotted in Figure 11. From Table IV and Figure 11 it can be observed that the performance of GD and GGD-based algorithms is not impacted much by changing the environment. It can be observed that the accuracy

TABLE III: Comparison of the proposed GD and GGD with SVM, DT, NB, and NN algorithms.

Algorithms	TPR	FPR	FNR	TNR	Precision	Recall	Accuracy	AUC
SVM	949	51	31	69	0.968	0.949	0.926	0.916
DT	952	48	31	69	0.968	0.952	0.928	0.923
NB	953	47	28	72	0.971	0.953	0.932	0.93
NN	961	39	11	89	0.989	0.961	0.955	0.957
GD	973	27	9	91	0.990	0.973	0.967	0.965
GGD	983	17	4	96	0.995	0.983	0.980	0.982

TABLE IV: Performance comparison of the two different environments.

Algorithm	Training Scenario	Testing Scenario	TP	FP	FN	TN	Precision	Recall	Accuracy	AUC
GD	Studio	Studio	973	27	9	91	0.990	0.973	0.967	0.965
GD	Studio	Room	964	36	11	89	0.987	0.964	0.956	0.96
GGD	Studio	Studio	983	17	4	96	0.996	0.983	0.98	0.982
GGD	Studio	Room	974	26	7	93	0.993	0.974	0.97	0.975

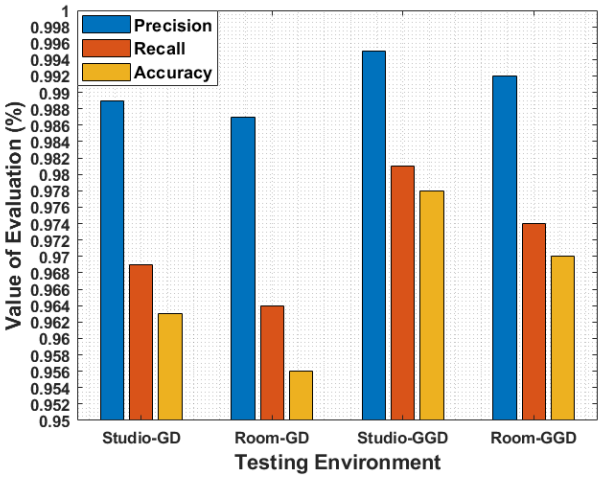

Fig. 11: Accuracy results of two different environments

of training in the studio and testing at room did not had a big impact. It can be observed from the figure and the table that the accuracy reduced by 0.011 and 0.01 when employing the GD- and GGD- based algorithm, respectively.

VII. Conclusions

In this paper, a featured-based method for the UWB localisation is proposed. The main aim is to improve the classification of the UWB IPS especially when the dataset is imbalanced, therefore, having a large number of LoS signals as compared to NLoS signals. Initially, in this work seven UWB signal components were collected, and based on these seven signal components, four key features were selected such as estimated distance, first path power level, received power level, and threshold power. With these key features, the joint probability densities for Gaussian and generalised Gaussian are calculated. In order to classify the LoS and NLoS signals a threshold is computed. From the simulation and experimental results, and it can be observed that the performance of the UWB localisation system was significantly improved by designing the GD and the GGD algorithms as compared to the existing SVM, DT, NB, and NN algorithms. The confusion matrix, ROC, and AUC area for these classification algorithms were compared. In addition, we computed the different ratios of LoS and NLoS signals in the dataset. It can be observed that the classification accuracy improves as the imbalance in dataset is removed, therefore, having same number of LoS and NLoS signals. Finally, from this paper, it can be concluded that the GGD algorithm is effective for NLoS signal identification with balanced Los-NLoS mixed data and remain highly accurate even if we have unbalanced data. For future work, the data can be extended to a large dataset with more signal features to evaluate the classification accuracy. Furthermore, the assumption that all the features are independent will also be removed.

References

[1] B. Pinto, R. Barreto, E. Souto and H. Oliveira, "Robust RSSI-Based Indoor Positioning System Using K-Means Clustering and Bayesian Estimation," in IEEE Sensors Journal, vol. 21, no. 21, pp. 24462-24470, 1 Nov.1, 2021.

[2] W. Jiang, Z. Cao, B. Cai, B. Li and J. Wang, "Indoor and Outdoor Seamless Positioning Method Using UWB Enhanced Multi-Sensor Tightly-Coupled Integration," in IEEE Transactions on Vehicular Technology, vol. 70, no. 10, pp. 10633-10645, Oct. 2021.

[3] Z. Wu, Y. Yue, M. Wen, J. Zhang, J. Yi and D. Wang, "Infrastructure-Free Hierarchical Mobile Robot Global Localization in Repetitive Environments," in IEEE Transactions on Instrumentation and Measurement, vol. 70, pp. 1-12, 2021.

[4] Y. Wu, R. Chen, W. Li, Y. Yu, H. Zhou and K. Yan, "Indoor Positioning Based on Walking-Surveyed Wi-Fi Fingerprint and Corner Reference Trajectory-Geomagnetic Database," in IEEE Sensors Journal, vol. 21, no. 17, pp. 18964-18977, 1 Sept.1, 2021

[5] L. Alsmadi, X. Kong, K. Sandrasegaran and G. Fang, "An Improved Indoor Positioning Accuracy Using Filtered RSSI and Beacon Weight," in IEEE Sensors Journal, vol. 21, no. 16, pp. 18205-18213, 15 Aug.15, 2021

[6] Q. Z. Ahmed, M. Hafeez, F. A. Khan and P. Lazaridis, "Towards Beyond 5G Future Wireless Networks with focus towards Indoor Localization," 2020 IEEE Eighth International Conference on Communications and Networking (ComNet), 2020, pp. 1-5, doi: 10.1109/ComNet47917.2020.9306084.

[7] I. M. Abou-Shehada, A. F. AlMuallim, A. K. AlFaqeh, A. H. Muqaibel, K. -H. Park and M. -S. Alouini, "Accurate Indoor Visible Light Positioning Using a Modified Pathloss Model With Sparse Fingerprints," in Journal of Lightwave Technology, vol. 39, no. 20, pp. 6487-6497, Oct.15, 2021

[8] Q. Pu, J. K. -Y. Ng and M. Zhou, "Fingerprint-Based Localization Performance Analysis: From the Perspectives of Signal Measurement and Positioning Algorithm," in IEEE Transactions on Instrumentation and Measurement, vol. 70, pp. 1-15, 2021.

[9] C. Wang, A. Xu, J. Kuang, X. Sui, Y. Hao and X. Niu, "A High-Accuracy Indoor Localization System and Applications Based on Tightly Coupled UWB/INS/Floor Map Integration," in IEEE Sensors Journal, vol. 21, no. 16, pp. 18166-18177, 15 Aug.15, 2021.

[10] S. Hayat, E. Yanmaz and R. Muzaffar, "Survey on Unmanned Aerial Vehicle Networks for Civil Applications: A Communications Viewpoint," in IEEE Communications Surveys & Tutorials, vol. 18, no. 4, pp. 2624-2661, Fourthquarter 2016.

[11] P. Chhikara, R. Tekchandani, N. Kumar, V. Chamola and M. Guizani, "DCNN-GA: A Deep Neural Net Architecture for Navigation of UAV in Indoor Environment," in IEEE Internet of Things Journal, vol. 8, no. 6, pp. 4448-4460, 15 March15, 2021.

[12] W. Wang, D. Marelli and M. Fu, "Multiple-Vehicle Localization Using Maximum Likelihood Kalman Filtering and Ultra-Wideband Signals," in IEEE Sensors Journal, vol. 21, no. 4, pp. 4949-4956, 15 Feb.15, 2021.

[13] C. T. Nguyen et al., "A Comprehensive Survey of Enabling and Emerging Technologies for Social Distancing—Part I: Fundamentals and Enabling Technologies," in IEEE Access, vol. 8, pp. 153479-153507, 2020.

[14] V. Chamola, V. Hassija, S. Gupta, A. Goyal, M. Guizani and B. Sikdar, "Disaster and Pandemic Management Using Machine Learning: A Survey," in IEEE Internet of Things Journal, vol. 8, no. 21, pp. 16047-16071, 1 Nov.1, 2021.

[15] N. Kbayer and M. Sahmoudi, "Performances Analysis of GNSS NLOS Bias Correction in Urban Environment Using a Three-Dimensional City Model and GNSS Simulator," in IEEE Transactions on Aerospace and Electronic Systems, vol. 54, no. 4, pp. 1799-1814, Aug. 2018.

[16] B. Hanssens et al., "An Indoor Variance-Based Localization Technique Utilizing the UWB Estimation of Geometrical Propagation Parameters," in IEEE Transactions on Antennas and Propagation, vol. 66, no. 5, pp. 2522-2533, May 2018.

[17] F. Che, A. Ahmed, Q. Z. Ahmed, S. A. R. Zaidi and M. Z. Shakir, "Machine Learning Based Approach for Indoor Localization Using Ultra-Wide Bandwidth (UWB) System for Industrial Internet of Things (IIoT)," 2020 International Conference on UK-China Emerging Technologies (UCET), 2020, pp. 1-4.

[18] W. B. Abbas, F. Che, Q. Z. Ahmed, F. A. Khan and T. Alade, "Device Free Detection in Impulse Radio Ultrawide Bandwidth Systems," Sensors, vol. 21, no. 9, pp. 1–19, Sept. 2021.

[19] L. Yan, Y. Lu and Y. Zhang, "An Improved NLOS Identification and Mitigation Approach for Target Tracking in Wireless Sensor Networks," in IEEE Access, vol. 5, pp. 2798-2807, 2017.

[20] K. Gururaj, A. K. Rajendra, Y. Song, C. L. Law and G. Cai, "Real-time identification of NLOS range measurements for enhanced UWB localization," 2017 International Conference on Indoor Positioning and Indoor Navigation (IPIN), 2017, pp. 1-7.

[21] A. Abolfathi Momtaz, F. Behnia, R. Amiri and F. Marvasti, "NLOS Identification in Range-Based Source Localization: Statistical Approach," in IEEE Sensors Journal, vol. 18, no. 9, pp. 3745-3751, 1 May1, 2018.

[22] Q. Tian, K. I. Wang and Z. Salcic, "An INS and UWB Fusion Approach With Adaptive Ranging Error Mitigation for Pedestrian Tracking," in IEEE Sensors Journal, vol. 20, no. 8, pp. 4372-4381, 15 April15, 2020.

[23] S. Maranò, W. M. Gifford, H. Wymeersch and M. Z. Win, "NLOS identification and mitigation for localization based on UWB experimental data," in IEEE Journal on Selected Areas in Communications, vol. 28, no. 7, pp. 1026-1035, September 2010.

[24] H. Wymeersch, S. Marano, W. M. Gifford and M. Z. Win, "A Machine Learning Approach to Ranging Error Mitigation for UWB Localization," in IEEE Transactions on Communications, vol. 60, no. 6, pp. 1719-1728, June 2012.

[25] B. Chitambira, S. Armour, S. Wales and M. Beach, "NLOS Identification and Mitigation for Geolocation Using Least-Squares Support Vector Machines," 2017 IEEE Wireless Communications and Networking Conference (WCNC), 2017, pp. 1-6.

[26] F.Che, A. Ahmed., Q. Z. Ahmed, and M. Z. Shakir," Artificial intelligence for localisation of ultra-wide bandwidth (UWB) sensor nodes, "In AI for Emerging Verticals: Human-Robot Computing, Sensing and Networking (2020 ed.). IET

[27] S. Krishnan, R. Xenia Mendoza Santos, E. Ranier Yap and M. Thu Zin, "Improving UWB Based Indoor Positioning in Industrial Environments Through Machine Learning," 2018 15th International Conference on Control, Automation, Robotics and Vision (ICARCV), 2018, pp. 1484-1488.

[28] Q. Zheng et al., "Channel Non-Line-of-Sight Identification Based on Convolutional Neural Networks," in IEEE Wireless Communications Letters, vol. 9, no. 9, pp. 1500-1504, Sept. 2020, doi: 10.1109/LWC.2020.2994945.

[29] J. Fontaine, M. Ridolfi, B. Van Herbruggen, A. Shahid and E. De Poorter, "Edge Inference for UWB Ranging Error Correction Using Autoencoders," in IEEE Access, vol. 8, pp. 139143-139155, 2020.

[30] Q. Z. Ahmed, K. Park and M. Alouini, "Ultrawide Bandwidth Receiver Based on a Multivariate Generalized Gaussian Distribution," in IEEE Transactions on Wireless Communications, vol. 14, no. 4, pp. 1800-1810, April 2015.

[31] Q. Z. Ahmed, L. Yang and S. Chen, "Reduced-Rank Adaptive Least Bit-Error-Rate Detection in Hybrid Direct-Sequence Time-Hopping Ultrawide Bandwidth Systems," in IEEE Transactions on Vehicular Technology, vol. 60, no. 3, pp. 849-857, March 2011.

[32] Q. Z. Ahmed and L. Yang, "Reduced-rank adaptive multiuser detection in hybrid direct-sequence time-hopping ultrawide bandwidth systems," in IEEE Transactions on Wireless Communications, vol. 9, no. 1, pp. 156-167, January 2010.

[33] C.L. Sang, B. Steinhagen, J. D. Homburg, M. Adams, M. Hesse, U. Rückert," Identification of NLOS and Multi-Path Conditions in UWB Localization Using Machine Learning Methods, " in Applied Sciences 2020, vol. 10, no. 11, pp. 3980-4005, June 2020.

[34] V. F. Miramá, L. E. Díez, A. Bahillo, and V. Quintero, "A Survey of Machine Learning in Pedestrian Localization Systems: Applications, Open Issues and Challenges," in IEEE Access, vol. 9, pp. 120138-120157, 2021.

[35] DW1000 User Manual [Online]. Available: https://www.decawave.com/sites/default/files/resources, (accessed on 23/05/2022).